Experimental and numerical investigation of abnormal combustion phenomena in high-performance hydrogen direct-injection engine operated in stochiometric conditions

Experimental and Numerical Investigation of Abnormal Combustion Phenomena in High-Performance Hydrogen Direct-Injection Engine Operated in Stochiometric Conditions

Authors: Piano, A., [a,*]; Rolando, L., [a]; Roggio, S., [a]; Millo, F., [a]; Tonelli, R., [b,*]; Gullino, F., [b]; Mortellaro, F. S., [b]

[a] Politecnico di Torino, Torino, Italy

[b] Ferrari Spa, Maranello, Italy

Corresponding authors: Andrea Piano, andrea.piano@polito.it; Roberto Tonelli, roberto.tonelli@ferrari.com

Abstract

Nowadays the use of Hydrogen (H2) within Internal Combustion Engine (ICE) represents a valuable solution also for high-performance applications since it allows carbon free combustion process preserving, at the same time, the driving experience of the engines fuelled with conventional fuels. On the other side, the low ignition energy and the high flammability range may lead to a high probability of abnormal combustion events especially at high engine loads. Therefore, this work aims at investigating the occurrence of knock and pre-ignition phenomena in a high-performance Direct Injection (DI) single cylinder Spark Ignition (SI) engine through the synergistic use of numerical simulations and experimental activities. A 3D-CFD model was calibrated against a set of experimental measurements. The engine model showed satisfactory predictive capabilities with a good matching with the experimental in-cylinder pressure traces. This virtual test rig was then used to investigate the impact of a different coolant temperature and different injector recess in terms of knock and pre-ignition tendency, and most of all, to define a robust simulation methodology to estimate the risk of hydrogen abnormal combustion events.

Keywords

Internal combustion engine; Hydrogen; Computational Fluid Dynamics; Abnormal Combustion; Pre-ignition; Knocking; Stoichiometric Conditions

1. Introduction

The huge climate changes observed in the last decades because of Greenhouse Gases (GHG) emissions boosted the efforts of the European Union (EU) to decarbonize its economy. Indeed, despite being responsible for less than 15% of the total CO2 emitted in the last 10 years, the EU, with the European Green Deal announced at the end of 2019 [1], declared its aim to achieve the carbon neutrality by 2050. In such a framework, the main goals concern the phase-out of the coal used for power generation and the reduction of methane emissions. Particular attention is also devoted to the shift toward more sustainable mobility since the road transportation sector is responsible for 18% of the total CO2 emissions and, differently from other relevant sectors (i.e. industry and buildings), has shown an increasing trend in the past 25 years [2]. Besides the fostering of powertrain electrification, the most promising solution for transport system decarbonization, the European Green Deal also supports the development and the production of sustainable alternative fuels capable to achieve a zero carbon impact in their entire life cycle [3]. Among them, hydrogen has recently become a highly attractive solution since it could be produced from renewable energy sources, and its combustion generates almost zero GHG emissions. Although H2 may be at first associated with Fuel Cell (FC) applications [4], presently the more commercialized approach, its use as fuel in internal combustion engines represents a very attractive option [5,6]. The advantages of hydrogen ICE compared to the FC technology include a higher tolerance to fuel impurities, flexibility to switch between fuels, reduction of rare materials usage and a lower thermal load to be managed. In addition, H2-ICE technology benefits from the reduced cost of using the existing manufacturing facilities and processes for conventional ICEs [7]. However, in order to successfully achieve the targets of an on-road sport car, the H2-ICE powertrain has to face demanding challenges: high specific power and torque, high revving capabilities, excellent transient response, and high efficiency at part load. The latter is usually not a high priority task for a sport car. However, due to its low density, H2 needs to be compressed for storage. Current standard storage pressure is 700 bar for passenger cars and light commercial vehicle. Nevertheless, such a high pressure does not allow to reach the same volumetric energy density of gasoline, which makes a reduced fuel consumption mandatory [8]. A further challenge for H2-ICE powertrain concerns the pollutant emissions management: although H2 is a carbon-free fuel, hydrogen combustion is characterized by emissions of nitrogen oxide (NOx) and traces of other pollutants (i.e., carbon monoxide (CO), carbon dioxide (CO2), hydrocarbons (HC), particulate matter (PM)) originated from the combustion of

lubrication oil [9]. In case of on-road sport car, the Aftertreatment System (ATS) must guarantee high conversion performance despite demanding boundaries conditions, such as high exhaust mass flow rate and a long distance between engine and ATS, which make the cold-start phases more challenging [10].

1.1 H2-ICE operating mode

H2-ICE can be operated with lean mixture thanks to the wide flammability range and high laminar flame speed of H2 [7]. Figure 1 shows qualitative trend of specific power, NOx, and efficiency of a H2-ICE as a function of lambda [8]. If ultra-lean mixtures are adopted (i.e., lambda > 2.8), the in-cylinder temperatures are sufficiently low as to avoid NOx formation and dedicated NOx aftertreatment should be avoided. Moreover, ultra-lean mixtures allow to significantly reduce the knock tendency, thus exploiting combustion anchor angles close to the optimum, but make the power density very low, creating also huge challenges for the design of charging system and Charge Air Cooler (CAC). By reducing the excess air, an increment of the specific power can be obtained thanks to a less demanding boost request. However, as lambda reduces, NOx emissions increase exponentially, peaking between lambda values of 1.2 and 1.3. Aftertreatment systems, originally designed for Diesel applications, can be adapted for use in H2-ICEs that operate under lean conditions (i.e. lambda > 1). HC, CO, and unburnt hydrogen can be oxidized using an Oxidation Catalyst (OC), while NOx and PM emissions can be treated using a Selective Catalytic Reduction (SCR) technology, applied to a particulate filter. Ammonia (NH3) emissions, resulting from the presence of a Urea injection system required by the SCR technology, can be treated by an Ammonia Slip Catalyst (ASC). However, the main constraint of this solution relies on packaging, as its dimensions depend on the flow rate of engine-out NOx. For a high-performance engine operating with a moderate lean mixture, excessively large aftertreatment system would be required due to very high engine-out NOx. Based on preliminary considerations, a maximum lambda of 2.2 is estimated for the utilization of this after-treatment system [8]. On the other hand, if stoichiometric mixture is exploited, NOx emission could be treated through a Gasoline like Three-way Catalyst (TWC), as demonstrated in [8], and the required boost pressure would be significantly lower. For these reasons, an experimental campaign was carried out to investigate lambda 1 operations on a high-performance 0.5L direct injection single cylinder spark ignition engine. However, the experiments showed that the power density achievable with such operating mode was significantly limited by abnormal combustion phenomena.

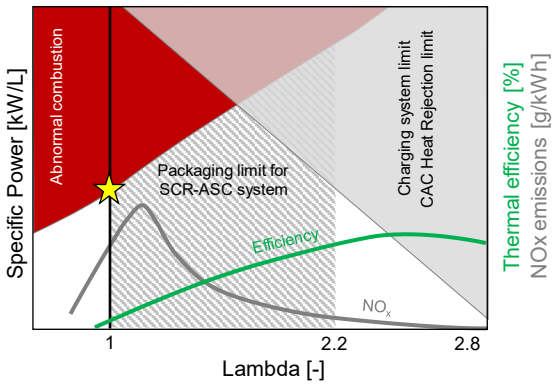

Figure 1. Schematic of hydrogen engine performance limits

1.2 Abnormal combustion

H2-ICEs, due to the combination of the hydrogen low minimum ignition energy and wide ignition limits, may face the following combustion anomalies:

- Knocking combustion;
- Pre-ignition.

Concerning knocking combustion, it refers to the self-ignition of the unburned mixture before it is reached by the flame front that takes place during the normal combustion process. It results in an abrupt heat release which produces a sudden increase of in-cylinder pressure, generating pressure oscillations inside the combustion chamber. These high-frequency pressure waves can mechanically stress or even damage the engine, and causes the engine structure to vibrate producing the familiar metallic knocking noise. This phenomenon is depicted in Figure 2 – a.

On the other hand, pre-ignition refers to the ignition of the air/hydrogen mixture before the spark timing. The starting points for pre-ignition are usually hot surfaces in the combustion chamber, the so-called "hot spots". Examples of this can be the spark plug electrodes, hot exhaust valves, sharp edges protruding into the combustion chamber, but also hot deposits or particles from lubricant. Mixture ignition can also occur because of residual discharge of the ignition system, also known as "phantom spark".

Pre-ignition phenomena can be divided as follows:

- Backfire: it involves combustion of the air-fuel mixture during the intake process. Ignition can take place either within the combustion chamber or by backflow of hot gases directly in the intake manifold. In this work, backfiring has been completely ruled out by exploiting a direct injection system and by performing the injection after inlet valve closure.
- Non knocking pre-ignition: as depicted in Figure 2 – b, the air-fuel mixture starts burning before spark timing, but the sequence is comparable to normal combustion process;
- Knocking pre-ignition: as depicted in Figure 2 – c, the air-fuel mixture starts burning before spark timing. The consequent combustion compresses and heats up the unburned charge which self-ignites. This type of pre-ignition very often leads to engine damage.

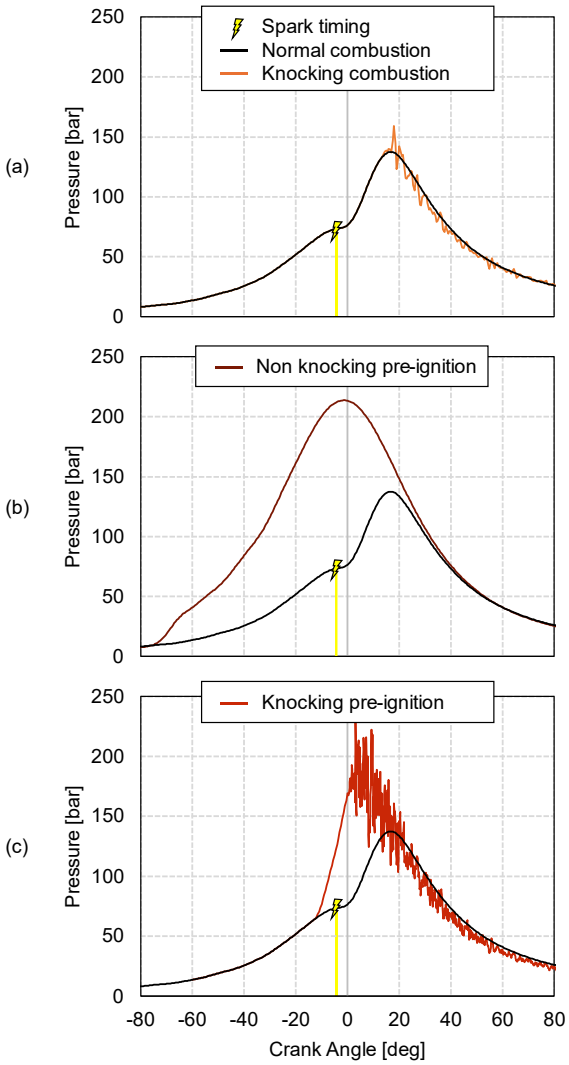

Figure 2. Example of normal combustion compared with different combustion anomalies (Knocking, Non knocking pre-ignition, Knocking pre-ignition). Engine operating condition: 6000 rpm x 24 bar IMEPH, lambda 1.

Each type of pre-ignition can in turn be classified as a function of its occurrence frequency. Runaway pre-ignition is characterized by a rapid acceleration of the ignition timing from cycle to cycle and a continuous increase in the maximum in-cylinder temperature and pressure. On the other hand, when the presence or absence of an ignition source is considered to change from cycle to cycle, pre-ignition is defined as sporadic [11–13].

In this framework, the aim of this work concerns the investigation of abnormal combustion phenomena in a high-performance Single Cylinder Engine (SCE) through the synergistic use of numerical simulations and experimental activities. In particular, a 3D-CFD model developed in the commercially available software CONVERGE was firstly calibrated against a preliminary set of experimental measurements. Afterwards, this virtual test rig was used to investigate the impact of a different coolant temperature and different injector recess in terms of knock and pre-ignition tendency, and most of all, to define a robust simulation methodology to estimate the risk of hydrogen abnormal combustion events.

2. Experimental analysis

2.1 Test engine

A dedicated experimental measurement campaign was performed on a 0.5L direct injection spark ignition SCE. The characteristics of engine under investigation, whose combustion chamber was derived from Ferrari 296GTB V6 Turbocharged engine, are presented in Table 1. The H2 injector was mounted in central position in the combustion chamber, while the spark plug was located in the region between the exhaust valves as in the production engine. The injector was specially designed and manufactured for low-pressure (i.e., 5 bar – 40 bar) direct injection of H2, with a mass flow equal to 10.5 g/s at 25 barA/85 °C. The injector includes a nozzle that opens outwards to prevent the in-cylinder pressure during the combustion from blowing back into the injector. Hydrogen was injected at a variable pressure through external pressure regulator connected directly to high pressure vessel, keeping constant the temperature equal to 25°C. In addition, piston, spark plug, and cylinder head were adapted for hydrogen combustion. A Variable Valve Timing (VVT) system was installed both on intake and exhaust camshafts. The combustion chamber was instrumented with a piezoelectric pressure transducer (Kistler 6045b) located between intake and exhaust valves on the side. During the experiments, 200

142 engine cycles were acquired for a reliable statistical analysis of the indicated data. More details about the test
143 case and experimental activity are available in previous works of the authors [8,14].

144 **Table 1**. Single Cylinder H2 Engine Specifications.

Displaced volume	498.7 cc
Stroke	82 mm
Bore	88 mm
Compression ratio	10.5:1
Number of Valves	4
H2 injector	Direct – Central Mounted
H2 Pressure	5 – 40 bar
Ignition	Exhaust side spark plug
Intake Cam lift	10.5 mm
Exhaust Cam lift	10.5 mm

145

146 **2.2 Results**

147 The experimental campaign consisted in three different load sweeps at the engine speed of 6000 rpm. As
148 described in Table 2, the first test (i.e., "Test #1") was carried out with a coolant temperature of 90°C and an
149 injector recess of Z = -1 mm. This test will be referred as the "baseline" configuration. In the second load
150 sweep, the coolant temperature was reduced up to 50°C without modifying the injector position (i.e., "Test
151 #2"); while the third test featured a coolant temperature of 90°C and an injector recess of Z = -3 mm (i.e., "Test
152 #3").

153 **Table 2**. Experimental tests specifications

Test	**Coolant Temperature [°C]**	**Injector Recess | Z [mm]**
#1	90	-1
#2	50	-1
#3	90	-3

154

155 To better clarify the notation adopted for the injector recess, Figure 3 qualitatively shows the position of the
156 injector for Test #1 and Test #3. In detail, injector recess Z = 0 mm corresponds to the injector tip aligned with
157 the cylinder head. In addition, negative values of the recess correspond to a position set back from the cylinder
158 head, as depicted in Figure 3.

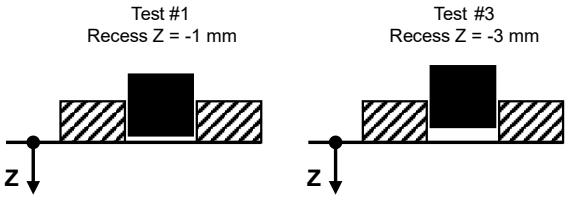

Figure 3. Injector recesses geometry.

In these experiments, the load was controlled through the intake pressure, while the mixture was kept in stoichiometric condition. H2 injection pressure was regulated in such a way to obtain an injection duration of 2 ms, corresponding to approximately 70 deg. The Start of Injection (SOI) was set at 140 deg bTDCf in order to exploit the benefits of late injection strategy [8], and the positions of the VVTs were held fixed. Spark timing was regulated at knock limit condition: the so-called Knock Limited Spark Advance (KLSA) was identified when the 99.5th percentile of Maximum Amplitude Pressure Oscillation (MAPO) exceeded a certain threshold [14]. For all the three tests, the load increment was always limited by the appearance of pre-ignition phenomena, as shown in Figure 2 – c. It is worth to highlight that the load sweeps were stopped when 1% of engine cycles presented pre-ignition.

Firstly, the impact of coolant temperature on combustion parameters and its anomalies was evaluated by comparing Test #1 and #2. Gasoline SI engine experience showed that knock is a temperature driven phenomenon, and since the lower coolant temperature reduces the end-gas reaction rate, this modification has a positive impact on knock occurrence [15]. This is also confirmed for H2 engines, as shown in Figure 4: Test #2 showed, indeed, more advanced crank angle at 50% of total Mass Fraction Burnt (MFB50) in comparison with Test #1 (~2.5 CAD on average). On the other hand, it is worth to point out that the tested coolant temperature reduction had negligible impact on pre-ignition occurrence.

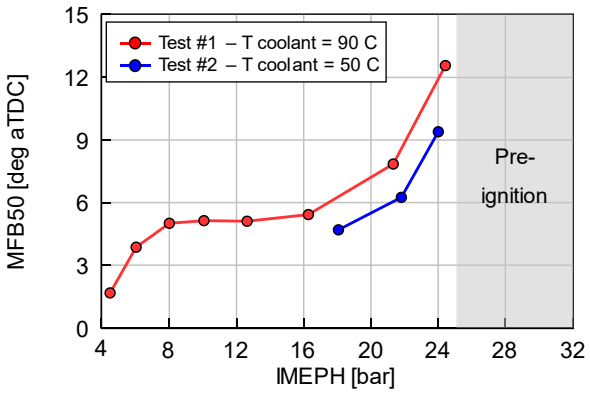

Figure 4. Engine load sweep at 6000 rpm. MFB50 at KLSA for different coolant temperatures.

Once assessed the impact of the coolant temperature, Test #3 moved the focus to the assessment of injector recess impact on combustion process. As shown in a previous work [16], the H2 injector recess highly influences jet penetration and width, with a relevant impact on hydrogen-air mixing. Similarly, the injector recess showed a relevant influence on pre-ignition phenomena: in fact, moving from Z = -1 mm (Test #1) to Z = - 3 mm (Test #3), the pre-ignition occurrence increased thus limiting the maximum IMEPH achievable (>2 bar difference between the two different recesses). Contrarily to coolant temperature test, injector position showed negligible impact on knock tendency, as highlighted in Figure 5, where similar MFB50 is adopted at KLSA for both injector recesses.

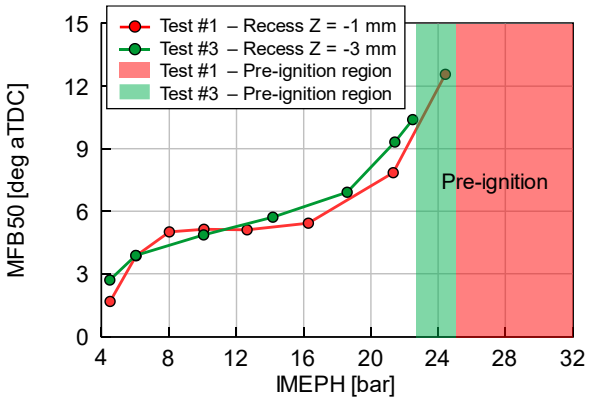

Figure 5. Engine load sweep at 6000 rpm. MFB50 at KLSA for different injector recesses.

3. Simulation analysis

3.1 Simulation setup and model validation

The commercially available software CONVERGE CFD v3.0.25 was used for the simulations. To properly initialize the computational domain, a 1D-CFD complete engine model was built in GT-SUITE, providing the time-dependent boundary conditions in terms of pressure, temperature, and species concentrations. A modified cut cell cartesian mesh with a base grid size of 4 mm was adopted. Then, fixed embeddings were included achieving 0.5 mm grid dimension close to the combustion chamber walls, 0.125 mm at spark location and up to 0.0625 mm at the H2 injector poppet valve. Further refinement has been achieved due to the Adaptive Mesh Refinement (AMR) technique [17], ensuring 0.25 mm-cell to capture not only the gas exchange through the intake/exhaust valves, but also the H2 mixing with fresh air, and subsequent combustion process. Figure 6

shows the mesh size distribution during the H2 injection: as abovementioned, specific refinement close to the injector and walls was coupled with the AMR activated by the velocity and temperature gradients.

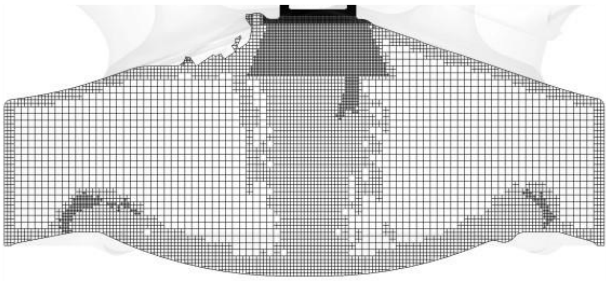

Figure 6. Mesh size during hydrogen injection.

The compressible form of RANS equations using RNG k-ε turbulence model was used to simulate the turbulent flow in the ICE [18]. The finite volume formulation of the equations was solved on the discretized domain, using second order central differences for spatial terms and implicit Euler scheme for the temporal term. The pressure-velocity coupling was done using PISO algorithm, and the Redlich-Kwong equation of state was used to close the system of equations. The mixture-averaged diffusion model was used to consider the high diffusivity of H2 in air, compared to heavy hydrocarbons. An adaptive time stepping algorithm was adopted where the solver determines the largest timestep that satisfy all the applicable limiters [17].

As far as combustion process is concerned, the Extended Coherent Flame Model (ECFM) was used to model the spark ignited combustion of H2 [17–19]. The advantage of using coherent flamelet models comes from the separation of combustion from the turbulent field. Such models work with the assumption that the reactions take place in a thin layer separating the burnt and unburnt gases [19]. The employment of this combustion model is justified by the reduced computational cost, as the number of scalar equations is smaller than in other models that make use of the detailed kinetic solver during the simulation. This is made possible by the short characteristic chemical time of hydrogen, which makes the flamelet assumption realistic, also considering the mixture composition condition (i.e., stoichiometric air-to-fuel ratio). This model solves a transport equation for the Flame Surface Density (FSD) which, along with the laminar flame speed, determines the fuel consumption rate. The interaction of the flame with the local turbulence is modelled using an addition source term for the turbulent stretch in the FSD equation. In the present study, the Intermittent Turbulent Net Flame Stretch (ITNFS) developed by [20] was used. The spark plug was modelled using the Imposed Stretch Spark Ignition Model (ISSIM) [21]. The ISSIM model helps in simultaneously simulating the electrical circuit energy

deposition and the flame surface and mass deposition [17]. The auto-ignition was modelled using an additional source term in the FSD equation adopting the Tabulated Kinetics of Ignition (TKI) model based on detailed chemistry scheme. To tabulate the ignition delay and the reaction rate due to autoignition, the TKI model is designed to solve the 0D constant pressure reactors over a wide range of initial conditions. Also Laminar Flame Speed (LFS) tables were obtained through the exploitation of detailed chemistry scheme. More specifically, TKI and laminar flame speed tables were generated adopting the GRI Mech 3.0 (53 species, 325 reactions) [22], testing the mechanism over a wide range of pressures, temperatures, equivalence ratios and residual gas fraction, as reported in Table 3.

Table 3. TKI and LFS tables ranges for air-H2 mixture.

	Min	**Max**	**Step**
Pressure [bar]	10	150	10
Temperature [K]	500	1200	100
Equivalence ratio [-]	0.3	2	0.1
Residual gas fraction [-]	0	0.2	0.05

Since the numerical validation of the H2 injection spray against experimental test on constant volume vessel has been already reported in [14], in this paper the validation is focused only on the combustion process. Starting from a previously validated model for low-speed/low-load engine operating conditions (2000 rpm x 4.5 bar IMEPH) [14], the model was calibrated under high speed / high load engine operating conditions (6000 rpm x 24 bar IMEPH), adopting a lower turbulent stretch constant (0.5) in the FSD equation. This modification is in line with the work presented in [18], where lower turbulent stretch constant is required by increasing the engine load. Figure 7 shows the comparison between the numerical and experimental in-cylinder pressure and Heat Release Rate (HRR). A high accuracy level has been achieved, well matching both the combustion phasing and intensity.

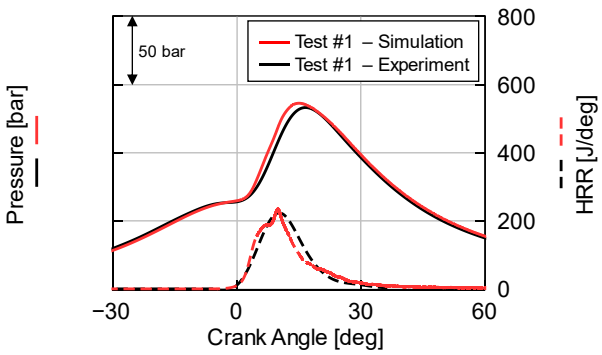

Figure 7. Model validation. In-cylinder pressure and HRR. Engine operating conditions: 6000 rpm x 24 bar IMEPH.

The calibrated model was then used to investigate the impact of a different coolant temperature and different injector recess in terms of pre-ignition tendency, and to define robust simulation methodology to estimate the risk of hydrogen abnormal combustion events.

3.2 Sensitivity analysis on coolant temperature

To investigate the abnormal combustion likelihood and the impact of the operating conditions on the abnormal propagation of the flame, experimental Tests #1 and #2 were considered (see Figure 4). As already discussed, no remarkable benefit was achieved in terms of pre-ignition resistance by reducing the coolant temperature, while the lower in-cylinder temperature led to an increment of the knock margin thus allowing a further advance of the combustion (~2.5 deg) at 6000 rpm x 24 bar IMEPH. To investigate this phenomenon in the 3D-CFD environment, the previously validated model was modified, reducing the walls temperature in the combustion chamber accordingly with the experiments. The results in terms of in-cylinder pressure and HRR are reported in Figure **8** – top. At fixed spark timing, reducing the wall temperatures leads to a retarded combustion due to the lower in-cylinder temperature distribution that affects the flame speed. Once assessed the effect on the combustion phenomenon, the auto-ignition tendency was investigated selecting the fuel reaction rate due to autoignition (i.e., omega TKI) as the most informative output variable. More in details, the omega TKI is computed starting from the reaction rate due to autoignition of the TKI table, thus being a function of pressure, unburned temperature, mixture composition and dilution of each cell within the fluid domain [23]. The omega TKI is computed for each computational cell with the unit (1/s). Then the global omega TKI within the combustion chamber is weighted for the mass of each cell, resulting in the global fuel reaction rate due to autoignition (mg/s). The omega TKI evolution is shown in Figure **8** – bottom for both coolant temperatures under investigation: pre-ignition was not observed for both the investigated coolant temperature as highlighted by the omega TKI values close to zero before the start of combustion. Moreover, it is worth to point out that the lower wall temperature case shows a reduced auto-ignition tendency (lower omega TKI), being in line with experimental data, in which the reduced temperature allowed an advanced combustion phasing thanks to a higher knock margin.

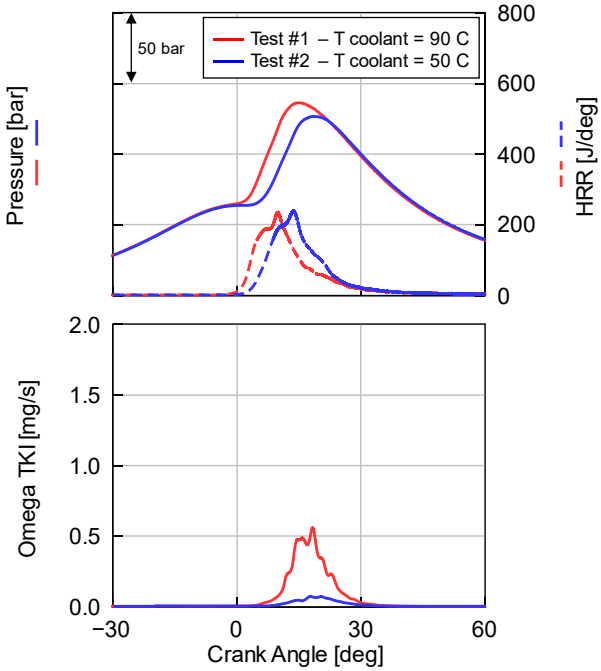

Figure 8. Sensitivity analysis on coolant temperature. Top: In-cylinder pressure and HRR; bottom: omega TKI. Engine operating conditions: 6000 rpm x 24 bar IMEPH.

To further understand the impact of coolant temperature on the knock likelihood, the approach proposed by Ando et al. in [24] was implemented. This approach selects the maximum of the omega TKI profile as a variable to quantify the knock tendency. More specifically, once defined the maximum of omega TKI at Knock Limited Spark Advance, each operating condition highlighting a higher value of omega TKI can be considered as knocking condition. Therefore, a spark advance sweep was simulated for both the operating conditions, and the results are presented in Figure 9, in which the maximum value of omega TKI is reported as a function of combustion anchor angle (i.e., MFB50). In addition, the "knock limit" dashed line represents the omega TKI value at the experimental KLSA. As expected, advancing the combustion phasing, a higher auto-ignition tendency was obtained, thus increasing the risk of abnormal combustion for both the cases under investigation. Interestingly, the lower coolant temperature shows reduced auto-ignition tendency as highlighted not only from the reduced omega TKI values, but also from the different trend slope. This confirms the experimental findings where reduced coolant temperature gave further margin on knock, thus allowing a more advanced combustion phasing.

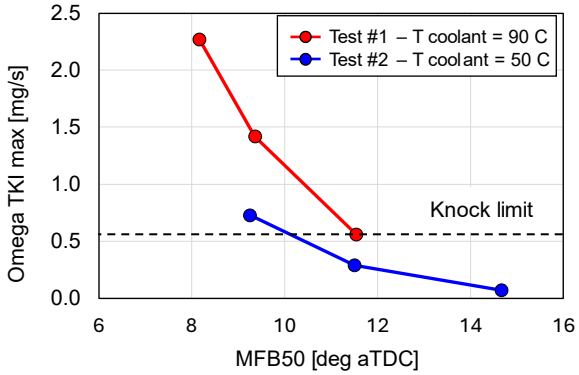

Figure 9. Sensitivity analysis on coolant temperature. MFB50 vs maximum of omega TKI over a spark timing sweep. Engine operating conditions: 6000 rpm x 24 bar IMEPH.

To quantify this effect, a further step in the model validation is presented in Figure 10, in which the MFB50 at KLSA obtained from simulations was compared with the experimental data for both the coolant temperatures under investigation. It is worth noting that the comparison between the numerical and experimental data shows a very good agreement, confirming that the numerical model is able to capture the reduced auto-ignition tendency induced by the lower coolant temperature. More in details, at KLSA the 3D-CFD model predicts a slightly lower combustion phasing advance than the one observed during the experiments ($\Delta MFB50_{exp} = 2.5\ deg; \Delta MFB50_{sim} = 1.5\ deg$).

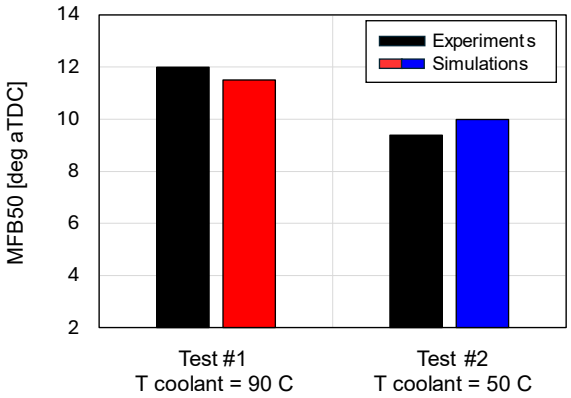

Figure 10. Model validation. MFB50 over different coolant temperatures. Engine operating conditions: 6000 rpm x 24 bar IMEPH.

3.3 Sensitivity analysis on injector recess

Not only the impact of coolant temperature, but also the one derived from different hydrogen injector recesses on pre-ignition likelihood has been investigated. Specifically, two different injector recesses were analysed in 3D-CFD environment (the reference Z = -1 mm and higher injector recess Z = -3 mm), with the aim of

developing a robust numerical methodology to investigate the risk of pre-ignition. As previously described, the experimental campaign highlighted a higher pre-ignition tendency by increasing the injector recess, thus limiting the maximum engine load up to 22 bar IMEPH at 6000 rpm. Instead, the reference Z = -1 mm reached 24 bar IMEPH without showing abnormal start of combustion. Therefore, both the injector recesses were analysed in 3D-CFD at the same engine operating conditions (6000 rpm x 24 bar IMEPH), where the pre-ignition was experimentally observed only for Z = -3 mm.

Firstly, the impact of the injector recess on the mixing process was investigated. To globally characterize the hydrogen-air mixing process within the combustion chamber, the equivalence ratio distribution at spark timing was analysed, as depicted in Figure 11. The total cylinder mass was binned by equivalence ratio into twenty intervals, starting from 0÷0.2 bin that corresponds to pure ambient gas and going up to 2 representing the rich mixture. As can be noted from Figure 11, the higher injector recess (i.e., Z = -3 mm) shows a higher peak of the distribution, thus suggesting a faster air/fuel mixing thanks to the faster jet penetration, as also highlighted in [16]. In addition, the mode of the distribution is closer to the target equivalence ratio (i.e., stoichiometric), while a reduced cylinder mass fraction can be observed in the tails of the distribution, thus confirming the enhanced mixing process induced by the higher injector recess.

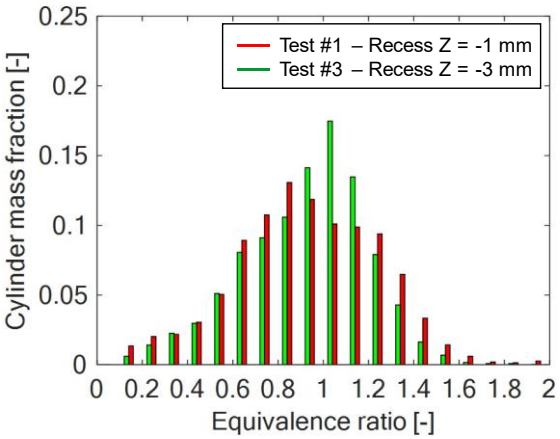

Figure 11. Equivalence ratio bins distribution over different injector recess at spark timing. Engine operating conditions: 6000 rpm x 24 bar IMEPH.

To further investigate the mixing process for both the injector recesses, the lambda and temperature local distribution at spark timing are depicted in Figure 12 and Figure 13, respectively. Two different cutting planes were considered for the scope: “Plane a” is perpendicular to the cylinder axis, while “Plane b” cuts the combustion chamber along the cylinder axis. Considering the lambda distribution in the Plane a of Figure 12

– top, the two injector recesses lead to different mixing processes: the Z = -3 mm injector recess shows a more homogeneous lambda distribution, and the leaner zone highlighted by the blue region is confined to the liner region. On the other hand, the local temperature distribution in Figure 13 – top, clearly shows that the hotter areas correspond to the leaner zones in the exhaust valves region of Figure 12 – top. In other words, where the hydrogen is less mixed with air, a higher temperature of the mixture can be observed within the combustion chamber. This is due the under-expanded hydrogen jet that reaches lower temperatures than the surrounding air during the injection event [25], thus providing a cooling effect of the overall mixture. In particular, the more the mixing process is enhanced, the lower the mixture temperature. Same conclusions can be made by observing the Plane b distributions in Figure 12 – bottom and Figure 13 – bottom. In addition, this representation shows that high temperature lean zones are mainly localized under the exhaust valves, especially for Z = -3 mm injector recess.

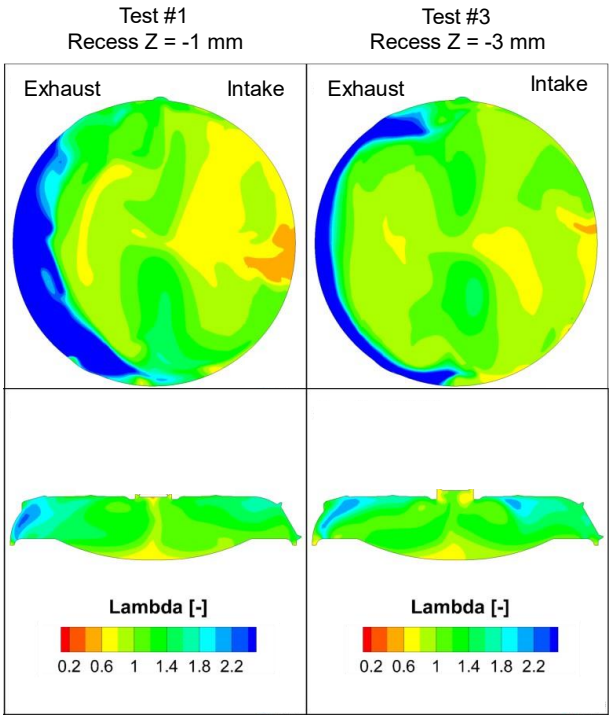

Figure 12. Lambda distribution over different injector recess at spark timing. Top: Plane a; bottom: Plane b. Engine operating conditions: 6000 rpm x 24 bar IMEPH.

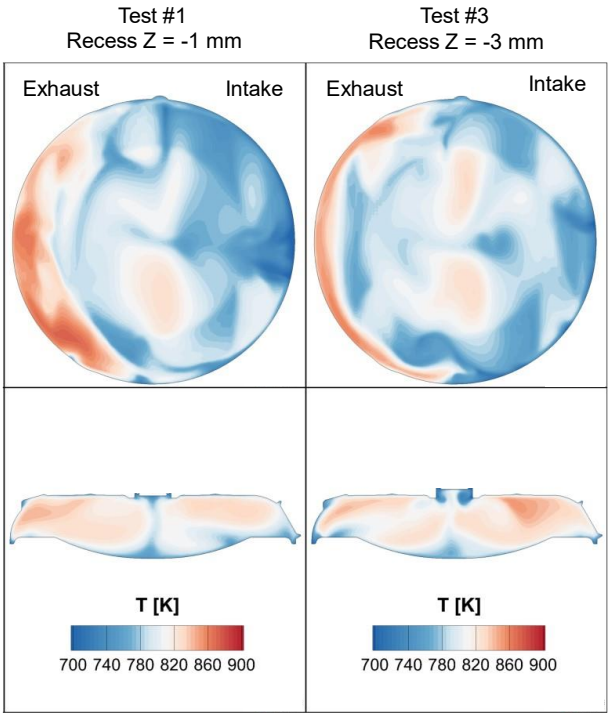

Figure 13. Temperature distribution over different injector recess at spark timing. Top: Plane a; bottom: Plane b. Engine operating conditions: 6000 rpm x 24 bar IMEPH.

Once investigated the effect of different injector recesses on the mixing process, the combustion simulations were carried out and the results in terms of in-cylinder pressure and HRR are reported in Figure 14 – top. At constant spark timing, increasing the injector recess results in faster combustion, mainly due to the enhanced mixing process that leads to a more homogeneous mixture and reduced lean regions which hinder the hydrogen flame propagation.

As already done for coolant temperature sensitivity analysis, the omega TKI evolution was selected as index for the auto-ignition tendency. Figure 14 – bottom shows a higher auto-ignition tendency for the increased injector recess in comparison with the baseline Z = -1 mm. This result suggests that increasing the mixture homogeneity does not necessarily lead to a normal flame propagation, that instead can be characterized by higher risk of auto-ignition of the end-gas. Nevertheless, both the omega TKI profiles show values close to zero before start of combustion, thus highlighting potential risk of knock without any pre-ignition events, differently from the experimental data.

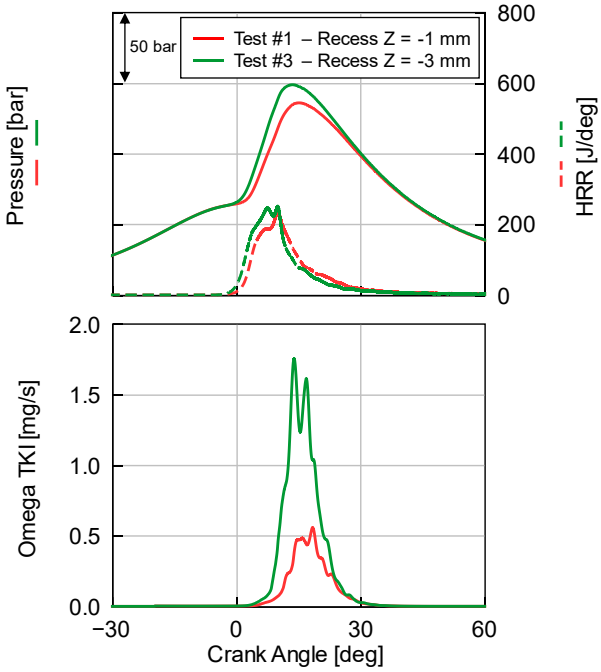

Figure 14. Sensitivity analysis on injector recess. Top: In-cylinder pressure and HRR; bottom: omega TKI. Engine operating conditions: 6000 rpm x 24 bar IMEPH.

Since the aim of this research activity was to define robust methodology to evaluate the pre-ignition tendency by means of numerical tools, the local distribution of the omega TKI within the combustion chamber was evaluated for both the injector recesses under investigation. The omega TKI, indeed, is the auto-ignition reaction rate from the TKI table and can be considered as index of the local chemical reaction rate. Figure 15 shows the omega TKI (top), lambda (center) and temperature (bottom) distributions at +1 Crank Angle Degree (CAD) after spark timing in the "Plane c" cutting plane, parallel to previously mentioned Plane a, but closer to the valves. In addition, the black line in the contour plots is representative of the iso-line at maximum omega TKI between the two cases under investigation. Considering the omega TKI in Figure 15 – top, the Z = -3 mm injector recess highlights a higher chemical reaction rate distribution.

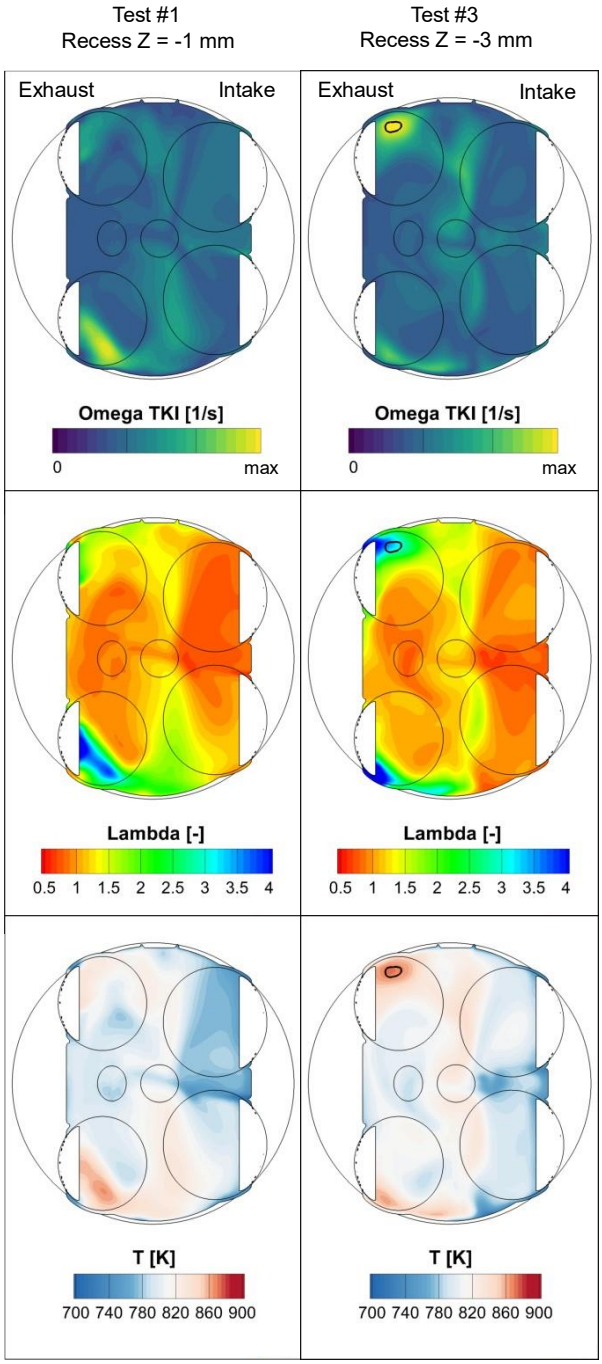

Figure 15. Sensitivity analysis on injector recess, at +1 CAD after spark timing. In-cylinder distribution over Plane c in terms of (top) omega TKI, (center) lambda and (bottom) temperature. The black line is representative of the iso-line at maximum omega TKI. Engine operating conditions: 6000 rpm x 24 bar IMEPH.

In particular, the top-left region below the exhaust valve is characterized by higher omega TKI values in comparison with the reference injector recess (Z = -1 mm). In this region, the maximum omega TKI is reached as highlighted by the black iso-line, that encloses a region in which the auto-ignition is prone to happen before the start of combustion. This can be due to a combined effect of the leaner mixture condition in the vicinity of the exhaust valve, where the wall temperature is high. In this region, indeed, the leaner lambda (Figure 15 –

center) leads to higher mixture temperature distribution (Figure 15 – bottom), thus promoting faster chemical reaction rate and higher risk of auto-ignition if compared with the baseline Z = -1 mm case.

To further investigate the pre-ignition likelihood, the values of lambda, temperature and omega TKI for each computational cell over the Plane c, at +1 CAD after spark timing, were analysed and depicted in Figure 16. Specifically, a scatter plot was defined considering the lambda value in the x-axis, and the gas temperature in the y-axis temperature. Each computational cell is represented by a single circle coloured by the value of the omega TKI, considering the same scale value adopted in Figure 15 – top. Moreover, both Z = -1 mm and Z = -3 mm cases are reported in Figure 16, top and bottom respectively. Starting from the results obtained considering the reference injector recess (Z = -1 mm) in Figure 16 – top, a higher omega TKI is observed for two regions. On one side, the richer lambda within the lambda 0.5-1 range provides an increment of omega TKI, and the richer the mixture the higher the omega TKI. However, the mixture temperature for those cells is low (i.e., <800 K) due to the limited air-hydrogen mixing, thus reducing the chemical reaction rate. On the other hand, for leaner lambda values (i.e., >2) the temperature is significantly increased due to the lower impact of the under-expanded hydrogen jet to the overall mixture temperature, thus increasing the value of omega TKI, reaching a maximum close to lambda 4. Then, moving to lambda values higher than 4, the reduced hydrogen content limits the chemical reaction rate and the omega TKI drops down. It is worth to point out that the mixture temperature does not increase as the mixture composition becomes more and more lean. This is mainly due to the impact of the heat transfer from the walls. As abovementioned, the resulting omega TKI distribution is a combination of two effects: on one side, the air-hydrogen mixing has a strong impact on the local temperature distribution due to the temperature difference between hot compressed air and under-expended hydrogen jet; but, on the other side, the local temperature distribution is also affected by the wall temperature, either enhancing or slowing down the chemical reactivity of the mixture.

Moving to the results for the injector recess Z = -3 mm in Figure 16 – bottom, a similar behaviour can be observed. Even for this injector recess, two regions show the higher omega TKI: the area with lambda 0.5-1 and temperature <800 K and the area with lambda >2. Also in this case, the maximum intensity of the omega TKI distribution is observed for lambda >2 due to the increased temperature. As expected, in this area the Z = -3 mm injector recess highlights a higher omega TKI intensity with respect to the reference injector recess and the maximum omega TKI value is located at lower lambda (i.e., equal to 3.5) in comparison with Z = -1 mm

case, as also shown in the top-left side of Figure 15. Conversely, the maximum omega TKI for the reference injector recess is shifted toward higher lambda (close to 4), that corresponds to the bottom-left side of Figure 15. In this zone, the high temperature level contributes to enhance the omega TKI, but the reduced hydrogen content (lambda equal to 4) limits this increment resulting in lower maximum omega TKI with respect to injector recess Z = -3 mm.

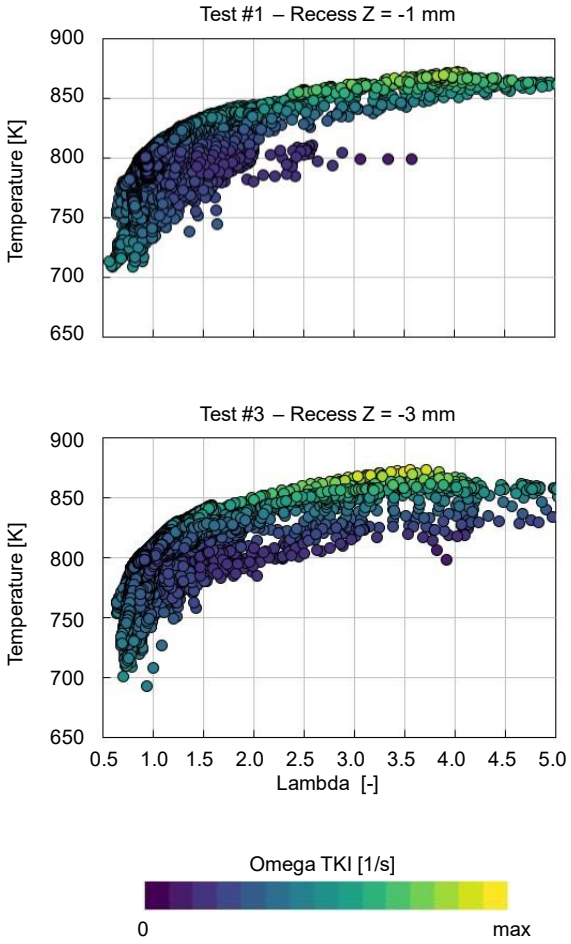

Figure 16. Lambda, temperature and omega TKI for each computational cell over Plane c, at +1 CAD after spark timing. Top: Recess = -1 mm; bottom: Recess = -3 mm. Engine operating conditions: 6000 rpm x 24 bar IMEPH.

In conclusion, even if the in-cylinder pressure predicted by 3D-CFD model did not highlight pre-ignition as observed in the experiments, a methodology to investigate the abnormal combustion risk has been developed and validated against the experimental data. The methodology relies on the outcomes of the numerical simulations and exploits the informative content of the omega TKI index, both in terms of average and local values, to predict pre-ignition risk, its location and knock likelihood.

It is worth to point out that a more refined solution of the boundary layer coupled with the Conjugate Heat Transfer (CHT) simulation can potentially make the methodology more reliable leading to more accurate temperature prediction close the walls; however this could remarkably increase the computational time required for the simulation activity.

4. Conclusions

This article presented a comprehensive methodology based on the synergistic use of numerical simulations and experimental activities to assess the occurrence of knock and pre-ignition phenomena in a 0.5L high-performance direct injection spark ignition single cylinder engine fuelled with hydrogen. At first, a dedicated experimental activity was carried out at 6000 rpm in stoichiometric mixture condition, during which the impact of injector recess and coolant temperature on abnormal combustion phenomena was assessed over different load levels. Afterwards, a 3D-CFD model developed in the commercially available software CONVERGE was calibrated under a high speed / high load engine operating conditions (6000 rpm x 24 bar IMEPH). This virtual test rig was then used to investigate the impact of a different coolant temperature on knock likelihood, showing a very good agreement with the experimental tests: indeed, the 3D-CFD model was able to capture the reduced auto-ignition tendency induced by the lower coolant temperature, predicting a combustion anchor angle advance of 1.5 deg rather than the 2.5 deg experimentally obtained. Successively, the engine model was exploited to assess the impact of a different H2 injector recess on pre-ignition propensity. In this case, even if the in-cylinder pressure predicted by the virtual engine featuring a higher injector recess did not highlight pre-ignition as observed in the experiments, the numerical tool was able to identify in-cylinder regions in which the auto-ignition is prone to happen before spark timing. To do so, a robust simulation methodology, which exploits the informative content of the average and local omega TKI index, was defined to estimate the risk of hydrogen abnormal combustion events.

Abbreviations

AMR	Adaptive Mesh Refinement
ASC	Ammonia Slip Catalyst
ATS	Aftertreatment System

bTCDf	before Top Dead Center firing
CAC	Charge Air Cooler
CAD	Crank Angle Degree
CFD	Computational Fluid Dynamics
CHT	Conjugate Heat Transfer
CO	Carbon Monoxide
CO2	Carbon Dioxide
DI	Direct Injection
ECFM	Extended Coherent Flame Model
EU	European Union
FC	Fuel Cell
FSD	Flame Surface Density
GHG	Greenhouse Gases
GRI	Gas Research Institute
H2	Hydrogen
HC	Hydrocarbon
HRR	Apparent gross Heat Release Rate
ICE	Internal Combustion Engine
IMEPH	Indicated Mean Effective Pressure - High
ISSIM	Imposed Stretch Spark Ignition Model
ITNFS	Intermittent Turbulent Net Flame Stretch
KLSA	Knock Limited Spark Advance
Lambda	Relative air-to-fuel ratio
LFS	Laminar Flame Speed
MAPO	Maximum Amplitude Pressure Oscillation
MFB50	50% Mass Fuel Burned angle
NH3	Ammonia
NOx	Nitrogen Oxide
OC	Oxidation Catalyst
PISO	Pressure-Implicit with Splitting of Operators
PM	Particulate Matter
RANS	Reynolds-Averaged Navier-Stokes
RNG	Re-Normalisation Group
SCE	Single Cylinder Engine
SCR	Selective Catalytic Reduction

SI	Spark Ignition
SOI	Start Of Injection
TKI	Tabulated Kinetics for Ignition
TWC	Three-way Catalyst
VVT	Variable Valve Timing
Z	Injector Recess

References

1. European Commission, "COMMUNICATION FROM THE COMMISSION: The European Green Deal," 2019, https://eur-lex.europa.eu/legal-content/EN/TXT/?uri=COM%3A2019%3A640%3AFIN, accessed July 2024.

2. Korn, T., "The Most Efficient Way for CO_2 Reduction: The New Generation of Hydrogen Internal Combustion Engines," 41st International Vienna Motor Symposium, 2020.

3. Dilara, P., "The Future of Clean Cars in Europe: EU Green Deal and EURO 7," 4th Sino-EU Workshop on New Emissions Standards and Regulations for Motor Vehicles, 2021.

4. Manoharan, Y., Hosseini, S.E., Butler, B., Alzhahrani, H., et al., "Hydrogen Fuel Cell Vehicles; Current Status and Future Prospect," Applied Sciences, 2019, 9(11):2296, https://doi.org/10.3390/app9112296.

5. Ghandhi, J., Günthner, M., and Novella, R., "Introduction to the current and future use of H2 and H2-based e-fuels in combustion engines and fuel cells Special Issue," *Int. J. Engine Res.*, 23(5):707–708, 2022, https://doi.org/10.1177/14680874221093003.

6. Nguyen, D. and Turner, J.W.G., "Towards carbon-free mobility: The feasibility of hydrogen and ammonia as zero carbon fuels in spark ignition light-duty vehicles," *Int. J. Engine Res.*, 1–65, 2024, https://doi.org/10.1177/14680874241239479.

7. Yip, H.L., Srna, A., Yuen, A.C.Y., Kook, S., et al., "A Review of Hydrogen Direct Injection for Internal Combustion Engines: Towards Carbon-Free Combustion," *Applied Sciences*, 9(22):4842, 2019, https://doi.org/10.3390/app9224842.

8. Medda, M., Calia, V., Di Sacco, M., Gullino, F., et al., “Challenges and Opportunities in developing a Hydrogen High Specific Power SCE in the roadmap towards zero net GHG,” 32nd Aachen Colloquium Sustainable Mobility 2023, 2023.

9. Wallner, T., Lohse-Busch, H., Gurski, S., Duoba, M., et al., “Fuel economy and emissions evaluation of BMW Hydrogen 7 Mono-Fuel demonstration vehicles,” *Int. J. Hydrogen Energy* 33(24):7607–7618, 2008, https://doi.org/10.1016/j.ijhydene.2008.08.067.

10. Rossi, V., Brocchi, L., Medda, M., Paltrinieri, S. et al., "Design and Assessment of an Exhaust After-Treatment System Equipped with a Fuel," SAE Technical Paper 2023-01-0355, 2023, https://doi.org/10.4271/2023-01-0355.

11. Takahashi, D., Matsubara, N., Yamashita, A., and Nakata, K., “Toyota‘s Hydrogen-Engine Development to Contribute to Carbon Neutrality,” 44th International Vienna Motor Symposium, 2023.

12. Grabner, P., Schneider, M., and Gschiel, K., "Formation Mechanisms and Characterization of abnormal Combustion Phenomena of Hydrogen Engines," SAE Technical Paper 2023-32-0168, 2023, https://doi.org/10.4271/2023-32-0168.

13. Rajasegar, R., Srna, A., Barbery, I., and Novella, R., "On the Phenomenology of Hot-Spot Induced Pre-Ignition in a Direct-Injection Hydrogen-Fueled, Heavy-Duty, Optical-Engine," Advances and Current Practices in Mobility 6(3):1535-1547, 2024, https://doi.org/10.4271/2023-32-0169.

14. Mortellaro, F., Silvestri, N., Zaffino, F., Medda, M. et al., "Effect of Start of Injection in a Hydrogen-Fueled DISI Engine: Experimental and Numerical Investigation," SAE Technical Paper 2023-24-0015, 2023, https://doi.org/10.4271/2023-24-0015.

15. Corrigan, D. and Fontanesi, S., "Knock: A Century of Research," SAE Int. J. Engines 15(1):57-127, 2022, https://doi.org/10.4271/03-15-01-0004.

16. Paltrinieri, S., Olcuire, M., Calia, V., Mortellaro, F. et al., "Experimental and Numerical Investigation of Hydrogen Injection and its Preliminary Impact on High Performance Engines Development," SAE Technical Paper 2023-01-0402, 2023, https://doi.org/10.4271/2023-01-0402.

17. Convergent Science, “CONVERGE Manual v3.0,” 2023.

18. Colin, O., Chevillard, S., Bohbot, J., Senecal, P.K., et al., "Development of a Species-Based Extended Coherent Flamelet Model (SB-ECFM) for Gasoline Direct Injection Engine (GDI) Simulations," Proceedings of the ASME 2018 Internal Combustion Engine Division Fall Technical Conference, Volume 2, 2018, https://doi.org/10.1115/ICEF2018-9684.

19. Colin, O., Benkenida, A., and Angelberger, C., “3D Modeling of Mixing, Ignition and Combustion Phenomena in Highly Stratified Gasoline Engines,” Oil & Gas Science and Technology - Rev. IFP, Vol. 58, 2003, https://doi.org/10.2516/ogst:2003004.

20. Meneveau, C., and Poinsot, T., "Stretching and quenching of flamelets in premixed turbulent combustion," Combustion and Flame, Volume 86, Issue 4, 1991, https://doi.org/10.1016/0010-2180(91)90126-V.

21. Colin, O., and Truffin, K., “A spark ignition model for large eddy simulation based on an FSD transport equation (ISSIM-LES),” Proceedings of the Combustion Institute, 33(2):3097–3104, 2011, https://doi.org/10.1016/j.proci.2010.07.023.

22. Gregory P. Smith, David M. Golden, Michael Frenklach, Nigel W. Moriarty et al., “GRI Mech 3.0,” http://www.me.berkeley.edu/gri_mech/, accessed July 2024.

23. Chevillard, S., Colin, O., Bohbot, J., Wang, M. et al., "Advanced Methodology to Investigate Knock for Downsized Gasoline Direct Injection Engine Using 3D RANS Simulations," SAE Technical Paper 2017-01-0579, 2017, https://doi.org/10.4271/2017-01-0579.

24. Ando, H., Shintani, Y., Kobayashi, H., Shiina, R. et al., "Study of Knocking Mitigation and Thermal Efficiency Enhancement of Pre-chamber Jet Combustion in Stoichiometric Gasoline Engine," SAE Technical Paper 2023-32-0006, 2023, https://doi.org/10.4271/2023-32-0006.

25. Hamzehloo, A. and Aleiferis, P.G., “LES and RANS modelling of under-expanded jets with application to gaseous fuel direct injection for advanced propulsion systems,” International Journal of Heat and Fluid Flow, 76:309–334, 2019, https://doi.org/10.1016/j.ijheatfluidflow.2019.01.017.

515